ENVIRONMENTAL STRESSES IN FLEXIBLY SUPPORTED BRIDGES

J. Leroy Hulsey, Assistant Professor of Civil Engineering,
North Carolina State University
Jack H. Emanuel, Professor of Civil Engineering, University of Missouri-Rolla

At present, no rational design method is available to account for movements and stresses in composite-girder bridges supported by flexible stub abutments. Because flexible stub abutments are frequently used, the objectives of this study were to: 1) develop a method for calculating environmentally induced movements and stresses and 2) compare the magnitude of these stresses induced in three types of construction for a 11-26-26-11-m (35-86-86-35-ft) four span six stringer composite-girder highway bridge located in mid-Missouri. Three types of support connections were investigated; 1) frictionless bearings, 2) non-integral end bents, and 3) integral end bents. Twenty years of recorded weather data were used for selection of upper and lower bound environmental loadings. Using these loadings as boundary conditions to the general heat flow equation, a finite element method was used to calculate resultant temperature distributions within a typical interior girder. These temperature distributions were then used as input to a slab-beam type element for calculation of the thermally induced stresses within the girder. Restraints imposed by the substructure, i.e. the bridge piers and earth embankments were modeled by linear springs. The results show that thermally induced stresses are significant for all three types of construction. Maximum beam stresses for the three supports were approximately 35%, 35%, and 52% of the allowable for frictionless bearings, non-integral abutments, integral abutments, respectively.

Bridge structures experience longitudinal movements and induced stresses which change continuously with time. The magnitude of movements and stresses induced by weather exposures is a function of the temperature distribution within the structure, the temperature at time of erection, material properties, geometry, support conditions, and structure flexibility (12, 15).

In conventional bridge design, expansive-contractive movements are generally assumed to be provided for by frictionless expansion bearings and by bridge deck expansion devices. Field observations show that bearings and expansion devices seldom function as anticipated. For example, Emanuel and Ekberg (5) reported numerous bridges with bearings that were tilted in the wrong direction, or frozen due to a build-up of grime, grit, and corrosion. They also reported a variety of problems associated with bridge deck expansion devices. When a conventional composite-girder bridge superstructure is supported by a massive or very stiff substructure, frozen bearings and/or inoperative expansion devices can cause excessive induced stresses. These stresses increase maintenance costs and lower the service life of the structure.

To reduce maintenance costs, some engineers have suggested connecting the superstructure to a flexible substructure. An 84 percent response to a survey of 50 state highway departments and 5 governmental agencies (6) showed that 28 respondents had used or were using this type of construction. The survey also showed that engineers are interested in using this type of construction, if rational design criteria are available to account for induced stresses.

Essentially, three types of superstructure to substructure connection details are being used by highway departments. Some states support the stringers on fixed rotational bearings which are attached to flexible piles at the abutments. This connection, commonly referred to as a "non-integral abutment," transfers shear forces to the piles. Other states encase the stringers in a monothlic pile cap which is referred to as an "integral abutment." This detail resists rotation and is assumed to transfer both shear and moment to the piles. Still other states use a detail that lies between the above two and is called a "semi-integral abutment." If the substructure is flexible enough, induced stresses may be provided for in the original design.

Although the composite-girder bridge superstructure supported by a flexible substructure appears to be a reasonable solution to the problem of a so-called maintenance free bridge, induced thermal stresses can present additional problems depending on structure length and substructure stiffness. Thus, the bridge engineer is faced with uncertainty as to the magnitude of stress induced by this type of construction and the behavior of the bridge over a period of time.

Previous studies of thermal and shrinkage

stresses in composite-girder bridge decks have been limited to bridges resting on frictionless bearings (4, 7, 19).

Zederbaum in 1966 (17) and 1969 (18) reviewed the factors affecting bridge deck movements in concrete bridges and presented a method for finding the location of the point of zero movement (stagnation point) on a bridge deck supported by elastic bearings. Witecki and Raina (16), 1969, presented a similar method to account for the effect of elastic and friction bearings on the point of zero movement and discussed the distribution of substructure forces and their application to the superstructure.

Bridge engineers are reluctant to use bridges supported by flexible substructures because design criteria are not currently available, observed data is limited, and guidelines relating substructure flexibility, bridge length, and induced stresses have not been developed.

As a first step towards the development of simple rational design criteria, the authors developed an analytical method as a basis for parametric studies. The procedure involved: a) evaluation of the factors affecting thermal properties of concrete; b) development of equations to estimate hourly weather extremes for Columbia, Missouri; c) formulation of a finite element method to solve the heat transfer equation which was used to find the temperature distribution through the bridge superstructure; d) development of a finite element method to find resultant thermal stresses; and e) a computerized solution of the magnitudes of thermally induced strains and stresses. Because of a space limitation and the complexity of the formulation, it is the objective of this paper to present results which show the potential magnitude of the maximum stresses induced by environmental loading extremes in an interior girder of a composite-girder bridge supported by a flexible substructure. Where necessary, for the benefit of the reader, an outline of the method is presented. No attempt was made to investigate the potential magnitude of stresses under combinations of dead, live, and environmental loads. The lengthy details of the initial development of these analytical procedures can be found in prior publications (7, 8, 9, 10, 12, 13).

Heat Flow

Generally, a bridge structure warms up during daylight hours due to the heat flux or energy received from the sun's rays. At night the structure cools down due to energy losses by convection and thermal radiation.

Physical Model

Consider a typical interior girder of the multi span composite-girder highway bridge of Fig. 1a. The heat flow through the superstructure produced by an environmental exposure fluctuates with time as a result of changes in air temperature, air velocity, and the solar radiation incident upon the structure.

Dividing the superstructure into long elements or members, m, each having constant sectional properties over the length, ℓ, assuming the concrete deck to be homogenous and isotropic and that the thermal properties are constant over the length of each member, the flow of heat through the member cross-section of Fig. 1b at some distance from the ends is essentially two-dimensional and is given by (12)

$$k\left(\frac{\partial^2 T}{\partial x^2} + \frac{\partial^2 T}{\partial y^2}\right) = c\rho \frac{\partial T}{\partial t} \qquad (1)$$

in which T is the temperature; x and y are cartesian coordinates; k is the thermal conductivity; c and ρ are the specific heat and density, respectively; and t is a point in time.

Figure 1. Heat flow model for a composite-girder bridge

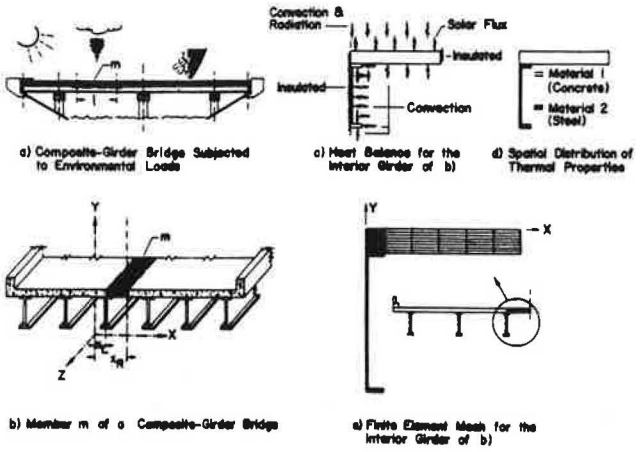

The initial condition, i.e. the temperature of the bridge structure at time of erection, is assumed to be at a steady state condition and is given by the mean daily temperature, T_a, for the day of the year when composite action is assumed to begin. Thus,

$$T(x, y, 0) = T_a \qquad (2)$$

At the air-deck (top) interface (Fig. 1c) energy is transferred by the solar flux absorbed by the bridge deck, $q_s(t)$, convection, $q_c(b,t)$, and thermal radiation, $q_r(b,t)$, such that

$$k\frac{\partial T}{\partial x}\ell_x + k\frac{\partial T}{\partial y}\ell_y + q_s(t) + q_c(b,t) + q_r(b,t) = 0 \qquad (3)$$

in which ℓ_x and ℓ_y are the direction cosines of the outward normal to the bridge deck and b represents the x, y coordinates on the boundary surface. At all other external boundary surfaces, such as the deck-air (bottom) interface and the girder-air interface, energy is assumed to be transferred by convection, and Eq. 3 reduces to

$$k\frac{\partial T}{\partial x}\ell_x + k\frac{\partial T}{\partial y}\ell_y + q_c(b,t) = 0 \qquad (4)$$

Physical Boundary Conditions

The solar radiation (heat gain) received by the deck can be expressed by $q_s(t) = \alpha I_n(t)$, in which α is the absorption coefficient and $I_n(t)$ is the sum of direct and diffuse radiation incident upon the surface.

Heat transfer by convection is given by Newton's Law of cooling

$$q_c(b,t) = h_c\{T(b,t) - T_\infty(t)\} \qquad (5)$$

in which h_c is a film coefficient, T(b,t) is the temperature of the bridge element at the surface-air temperature interface, and $T_\infty(t)$ is the air temperature at time t.

Heat transfer between the structure and the surrounding atmosphere due to thermal radiation (long) wave) produces a nonlinear heat flow boundary which can be modeled by (2, 14)

$$q_r(b,t) = \sigma\varepsilon\,[\theta(b,t)^4 - \varepsilon_{as}\theta_\infty(t)^4] \qquad (6)$$

where σ is the Stephan-Boltzman constant, ε is the emissivity, θ is the temperature in degrees absolute, and ε_{as} is the atmospheric emittance expressed in terms of air temperature as

$$\varepsilon_{as} = 1 - 0.261\,\exp\{-7.776 \times 10^{-4}\theta_\infty(t)^2\} \qquad (7)$$

in which $\theta_\infty(t)$ is in degrees centigrade.

Numerical Solution

The distribution of temperature through the cross section is obtained by solving the heat flow equation, Eq. 1, for the initial conditions of Eq. 2 and the boundary conditions of Eqs. 3 and 4. The geometric complexity and spatial distribution of the thermal properties, Figs. 1b and 1d, imply a need for a numerical method. A finite element method was developed, in which a typical interior slab-stringer was discretized as shown in Fig. 1e and the distribution of temperature was calculated at a given point in time. The formulation and details of the computional procedure are presented elsewhere (10, 12, 13)

Bridge Forces and Displacements

Forces induced by environmental exposures, shrinkage strains, and vehicular loads in an interior slab-stringer of a composite-girder bridge may be approximated by dividing the slab-stringer into prismatic elements connected by nodes; replacing the soil substrata, bearings and supporting structure with springs of equivalent stiffness; and using the stiffness method to solve for unknown displacements and forces.

Superstructure

Assuming an effective slab width, b_{ef}, consistent with present AASHO (now AASHTO) specifications (1), the slab-stringer shown in Fig. 2a is divided into composite-material slab-beam type elements, e, each having constant prismatic properties of length ℓ and defined by nodes i and j located at the neutral surface of the element. For the sign convention of Fig. 2c, the element stiffness matrix, $[k^e]$, is found by standard methods.

The total superstructure structural stiffness matrix, [K], i.e. without restraints imposed by the backfill and supporting structure, is obtained by assembling the element stiffness matrices.

The thermal fixed end forces for each element, $\{F_o^e\}$, at each nodal point and any superimposed nodal point loads, $\{P^L\}$, are assembled to give

$$\{P\} = \{P^L\} - \sum_{e=1}^{N_e} \{F_o^e\} \qquad (8)$$

where {P}, the vector of nodal point forces, is

$$\{P\} = [\,K\,]\,\{\Delta\} \qquad (9)$$

and {Δ} is the vector of unknown nodal point displacements.

Figure 2. Mathematical model for a restrained composite-girder bridge structure

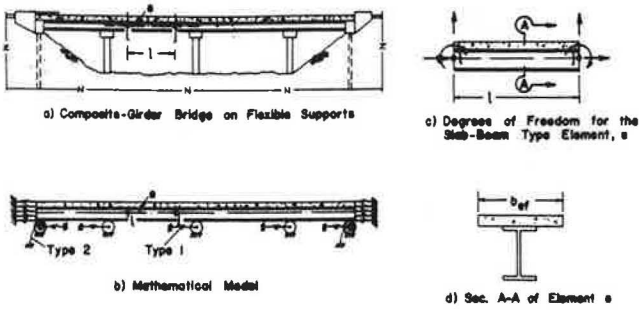

Substructure and Backfill

Restraint of longitudinal movements of a bridge deck induces both forces and moments in the bridge superstructure. For example, in bearing type supports a horizontal force is transferred through the bearing at some distance from the neutral surface, which induces a moment equal to the product of the force and its distance to the neutral surface. Integral or semi-integral abutments induce additional moment. Furthermore, both the approach slab and the fill material adjacent to the bridge deck will resist longitudinal movements. The magnitudes of the axial forces and the moments induced varies with the magnitude and distribution of the passive soil pressure resisting movement and the joint detail between the approach slab and the bridge deck.

Thus, two types of springs, shown in Fig. 2b, were used for analytically modeling the resistance of approach slabs, fills, abutment connections, and pier supports to superstructure movement.

The type 1 springs (one degree of freedom) were used to model bearing-pier supports, non-integral abutments, approach slabs, and fills adjacent to the bridge deck. The passive resistance of the fill material adjacent to the bridge deck is accounted for by applying multiple type 1 springs (winkler spring approximation), (see Fig. 2b). The type 2 springs are used to model the combined shear and moment resistance imposed by either the integral or semi-integral abutments.

Substructure and Backfill--Type 1 Springs

The spring force $^1F_{si,m}$ in spring m, attached to node i at $^1d_{si,m}$ from the neutral surface of the beam element, e, is given by

$$^1F_{si,m} = {}^1k_{si,m}\;{}^1\delta_{si,m} \qquad (10)$$

in which $^1k_{si,m}$ is the spring stiffness and $^1\delta_{si,m}$ is the spring displacement. Nodal point loads at node i of element e resulting from these spring forces are obtained by

$$\{^1P_{si,m}\} = \{^1H_{si,m}\}\;{}^1k_{si,m}\;{}^1\delta_{si,m} \qquad (11)$$

where $\{^1H_{si,m}\}$ is the force transformation matrix and $\{^1H_{si,m}\}^T$ is expressed by

$$\{^1H_{si,m}\}^T = \{\ 1 \quad 0 \quad -d_{si,m}\ \}$$

and $^1d_{si,m}$ is the distance from node i to spring m and is positive for springs located below the neutral surface.

The total nodal point forces, $\{Q_i\}$, at node i, which are located at the neutral surface of the slab-stringer element, are the sum of the nodal point loads, $\{P_i\}$, are the induced spring forces. This gives

$$\{Q_i\} = \{P_i\} + \sum_{m=1}^{^1S_i} \{^1P_{si,m}\}$$

in which $\{P_i\}$ is the summation of nodal point loads at node i; ^1S_i is the number of type 1 springs attached to node i; and $\{^1P_{si,m}\}$ is given by Eq. 11. Recognizing that the total nodal point forces, $\{Q_i\}$, at node i must be equal to the product of the assembled stiffness matrix at node i and the nodal point displacements at node i, it can be seen that

$$\{Q_i\} = [k_{ii}]\{\Delta_i\} = \{P_i\} - \sum_{m=1}^{^1S_i} \{^1H_{si,m}\}\ ^1k_{si,m}\ \ ^1\delta_{si,m}$$

Rewriting and transforming spring displacements, $^1\delta_{si,m}$ to the neutral surface of the slab-stringer element at each node gives

$$\{P\} = [\tilde{k}]\{\Delta\} \tag{12}$$

where

$$[\tilde{k}] = [k] + \sum_{i=1}^{^1N_s} \sum_{m=1}^{^1S_i} (\{^1H_{si,m}\}\ ^1k_{si,m}\ \{^1H_{si,m}\}^T) \tag{13}$$

Substructure--Type 2 Springs

The spring forces at node i are given by

$$\{^2F_{si}\} = [^2k_{si}]\{^2\delta_{si}\} \tag{14}$$

Transforming the spring forces from the spring to node i gives

$$\{^2P_{si}\} = [^2H_{si}]\ [^2k_{si}]\ \{^2\delta_{si}\} \tag{15}$$

where $[^2H_{si}]$ is the force transformation matrix and $[^2H_{si}]^T$ is expressed by

$$[^2H_{si}]^T = \begin{bmatrix} 1 & 0 & -^2d_{si} \\ 0 & 0 & 1 \end{bmatrix}$$

Similarly, as for the type 1 springs, the spring displacements are transformed to the neutral surface at each node and assembled to give

$$\{P\} = [\tilde{k}]\{\Delta\} \tag{16}$$

where

$$[\tilde{k}] = [\tilde{k}] + \sum_{i=1}^{^2N_s} ([^2H_{s_i}]\ [^2k_{s_i}]\ [^2H_{s_i}]^T)$$

After applying boundary conditions to Eq. 16, and rearranging, the nodal point displacements are obtained by

$$\{\Delta\} = [\tilde{k}]^{-1}\{P\} \tag{17}$$

Substructure Forces and Displacements

The pertinent displacements in the fill, approach slab and bearing supports are given by

$$^1\delta_{si,m} = [^1H_{si,m}]^T\ \{\Delta_i\} \tag{18}$$

Similarly, integral or semi-integral end bent displacements are given by

$$\{^2\delta_{si}\} = [^2H_{si}]^T\ \{\Delta_i\} \tag{19}$$

and the corresponding forces in each of the two types of springs are calculated by Eqs. 10 and 14 for types 1 and 2, respectively.

Substructure Stiffness Determination

Bearings

Three basic types of bearings are shown in Fig. 3: a fixed rotational bearing, a friction bearing, and an elastic bearing.

Figure 3. Flexibility coefficients for a bridge supporting structure

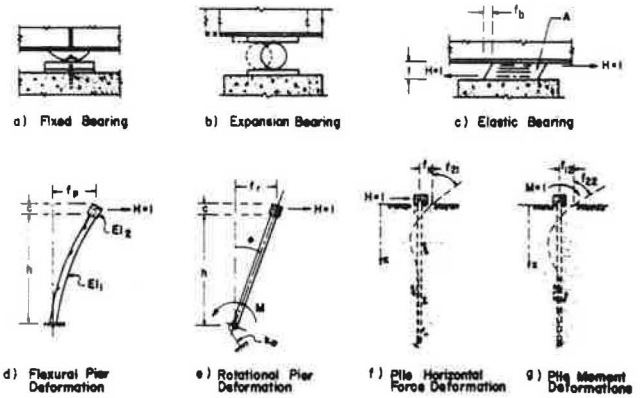

Fixed bearings, such as the curved steel plate of Fig. 3a, do not translate. Thus, the entire superstructure movement is transferred through the bearing to the support and the bearing flexibility, f_b, is

zero.

Friction bearings (Fig. 3b) perform like fixed bearings until a horizontal force equal to $\mu_s R$ produces impending motion. The coefficient of static friction, μ_s, for dry steel on steel varies from 0.15 to 0.8 (3, 11); R is the vertical reaction. After motion impends the resistance to movement (kinetic friction) is approximately three-fourths the static friction and the bearing resistance becomes $0.75\ \mu_s R$.

Elastic bearings, unlike the other two types, restrain movement and deform at the same time. From Fig. 3c, if a unit load is applied at the top of the bearing and the pier is restrained against movement, the resulting flexibility coefficient, f_b, becomes

$$f_b = \frac{t}{AG} \tag{20}$$

Piers

The pier flexibility (Fig. 3d), assuming elastic action, is found by applying a lateral unit load at the top of the pier. The resulting horizontal deflection or flexibility, f_p, is

$$f_p = \left(\frac{h^3}{3EI_1} + \frac{h^2 c}{2EI_2}\right) + \frac{c^3}{3EI_2} \tag{21}$$

From Fig. 3e, the rotation of the pier base may be accounted for by applying a lateral unit load at the top of a rigid pier. The resulting rotational deflection at the top of the pier, f_r, becomes

$$f_r = \frac{(h+c)^2}{k_\theta} \tag{22}$$

where k_θ may be found from the foundation type and the modulus of the soil.

Summing the individual flexibilities, $f = f_b + f_p + f_r$, for the total deflection at the top of the pier, and inverting gives the final effective pier stiffness (type 1 Spring) which is

$$k_s = \frac{1}{f} \tag{23}$$

where

1. For a fixed bearing pier, the total flexibility becomes

$$f = f_p + f_r = \left(\frac{h^3}{3EI_1} + \frac{h^2 c}{2EI_2}\right) + \frac{c^3}{3EI_2} + \frac{(h+c)^2}{k_\theta}$$

2. For a friction bearing, the flexibility is that of a fixed bearing when the horizontal thrust is equal to or less than $\mu_s R$, which gives

$$f = f_p + f_r = \left(\frac{h^3}{3EI_1} + \frac{h^2 c}{2EI_2}\right) + \frac{c^3}{3EI_2} + \frac{(h+c)^2}{k_\theta}$$

After motion impends the total flexibility of the pier is

$$f = \infty$$

3. For an elastic bearing the pier flexibility becomes

$$f = f_b + f_p + f_r = \frac{t}{AG} + \left(\frac{h^3}{3EI_1} + \frac{h^2 c}{2EI_1}\right) + \frac{c^3}{3EI_2} + \frac{(h+c)^2}{k_\theta}$$

Abutments

The governing differential equation for interaction between the surrounding soil and embedded piles subjected to lateral loads is

$$\frac{d^4 y}{dx^4} + \frac{ky}{EI} = 0 \tag{24}$$

where y is the lateral pile deflection, x is the depth below the top of pile, EI is the flexural pile stiffness, and k is the subgrade modulus in force/length^2.

For an assumed constant elastic soil modulus, classical solutions to Eq. 24 are readily available. For design conditions, the modulus may vary and numerical techniques are needed. Assuming an initial soil tangent modulus, i.e., small deformations, the flexibility of the pile supports may be evaluated by applying a unit lateral force and a unit moment at the top of the abutment pile as shown in Fig. 3f and 3g. Thus, taking into account the bearing type and applying the principles used for piers, the effective abutment stiffness can be found by inverting the flexibility matrix.

Superstructure Stress Analysis

Consider an interior composite slab-stringer to be subjected to thermal strains. In the composite section, a biaxial stress state exists at the interface between the slab and the beam flange. The state of stress depends on the imposed strain distribution, shear connector spacing, diaphragm and stringer spacing and support restraints. Previous analytical methods for the analysis of interior girders acting compositely with the slab are limited to frictionless bearing supports and have neglected transverse strain compatibility at the slab stringer interface (4, 6, 19).

In the method described herein, the bridge is first divided into composite-material slab-beam type elements, e, each having constant prismatic properties and a length of ℓ (see Fig. 4). Within each element, e, the assumptions made are: 1) the (one-way) slab and the beam are continuously connected by shear connectors; 2) the materials are homogenous and isotropic; 3) the temperature is constant over the length, ℓ, but may vary through the cross-section; 4) each girder is straight with a symmetrical cross-section; 5) elastic small deflection theory is valid; 6) torsional forces and transverse strain compatibility between separated slab sections are neglected; and 7) vertical strain compatibility is neglected.

Initially, the slab, upper beam flange and the top of the beam web are assumed separated and free to deform independently under the imposed temperature distribution and the resultant thermal strains are determined. Unrestrained thermal stresses within each separated section, n, are given by

$$\sigma'x_n = \frac{\alpha_n E_n}{\gamma}\left[-T(y_n) + \frac{1}{A_n}\int w_n\, T(y_n)\, dy_n + \frac{y_n}{I_n}\int w_n\, T(y_n)\, y_n\, dy_n\right] \tag{25a}$$

$$\sigma'y_n = 0 \quad ; \quad \sigma'z_n = \psi\sigma'x_n \tag{25b, 25c}$$

in which subscript n implies the appropriate separated section (Fig. 4), α_n is the coefficient of thermal expansion, E_n is the elastic modulus, T_n is the change in temperature, w_n is the width, A_n is the area, and I_n is the moment of inertia of each separated section. For plate action in the slab and top flange, $\gamma=1-\mu_n$ and $\psi=1$. Assuming the web and lower flange to be in place stress, $\gamma=1$ and $\psi=0$. The resulting unrestrained thermal strains are obtained from the general elasticity equations. For composite action, the slab and beam must deform with equal strains and curvatures at the interface. If one way slab action is valid, then the interface force system of unknown shears and couples of Fig. 4 must be superimposed. The eight unknown forces F_1 to F_8 are obtained by writing eight strain or curvature interface compatibility equations to yield eight simultaneous equations in eight unknowns. The details for this development have been presented in a separate publication (12).

Figure 4. Compatibility forces for superstructure components in a composite-girder bridge.

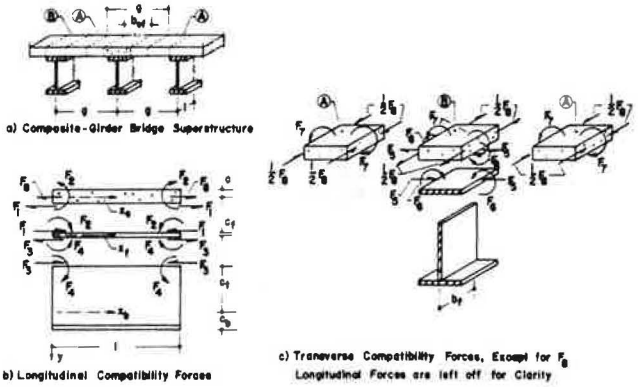

Final Stresses

Final stresses, forces and deformations for the interior slab-stringers of multi-span composite girder bridges subjected to thermal, shrinkage, or initial strains are obtained by superimposing the elastic stresses and the compatibility stresses.

Elastic stresses due to element forces are evaluated by a) dividing the slab-stringer into elements, b) introducing rigid boundaries at the nodal points, c) finding the fixed forces due to the deformations resulting from the thermal stresses of Eq. 25 and the stresses produced by F_1 to F_8, d) formulating the stiffness matrix, e) solving the resulting system of equations for nodal point displacements, and f) obtaining the element end forces and the resulting elastic stresses within the element.

Compatibility stresses are obtained by superimposing thermal stresses within the unrestrained and separated slab, beam flange, beam web and lower flange with the stresses produced by the compatibility forces, F_1 to F_8. Compatibility stresses within a determinate element are final stresses.

Point of Zero Movement

As expansive-contractive movements occur, a unique point on the bridge deck does not move. This point, when located, provides the engineer a rational means for determination of potential movement and placement of expansion joints, if used. Longitudinal displacements at the top surface of the bridge deck are obtained by transferring element nodal point displacements at the neutral surface to the top surface. Top surface strains at intermediate points along the element length can be calculated and used to numerically integrate and obtain axial deformations within each element. These deformations will change sign adjacent to the point of zero movement.

Bridge Study

A typical interior slab-stringer of a 11-26-26-11-m (35-86-86-35-ft) four span composite-girder six stringer highway bridge located in mid-Missouri was investigated for stresses induced by concrete shrinkage strains of 0.0002 and thermal strains resulting from air temperature extremes during the twenty year period of 1946-1965. An air entrained limestone aggregate concrete, for which the coefficient of thermal expansion is approximately 7.2×10^{-6}/°C (4.0×10^{-6}/°F), was assumed for the deck (8). The stringers are supported by flexibile stub abutments (semi-integral), a fixed bearing at the center pier and expansion bearings at intermediate piers. Pertinent superstructure properties are shown in Table 1.

Table 1. Bridge Properties

Type	Value
a) Superstructure	
Concrete compressive strength, kN/m² (psi)	27,600 (4000)
Effective slab width, mm[a] (in.)	1981 (78)
Slab thickness, mm (in.)	191 (7.5)
Depth of girder web, mm (in.)	1067 (42)
Section 1:	
Flange width and thickness, mm (in.)	203, 16 (8, 0.625)
Web thickness, mm (in.)	11 (0.4375)
Section 2:	
Top flange width and thickness, mm (in.)	203, 16 (8, 0.625)
Web thickness, mm (in.)	10 (0.375)
Bottom flange width and thickness, mm (in.)	254, 22 (10, 0.875)
Section 3:	
Flange width and thickness, mm (in.)	330, 25 (13, 1)
Web thickness, mm (in.)	11 (0.4375)
b) Substructure	
Concrete compressive strength, kN/m² (psi)	20,700 (3000)
Three-Column Expansion Piers:	
Pier cap width and height, m (ft)	0.84, 0.97 (2.75, 3.19)
Column diameter, mm (in.)	762 (30)
Column height, m (ft)	5.5 (18.1)
Bearing height, mm (in.)	241 (9.5)
Three-Column Fixed Pier:	
Pier cap width and height, m (ft)	0.84, 1.1 (2.75, 3.62)
Column diameter, mm (in.)	762 (30)
Column height, m (ft)	5.48 (17.96)
Bearing height, mm (in.)	102 (4)

[a]Neglects the top 25.4 mm (1 in.) of the slab.

The abutments are each supported by 5 HP 10 x 42 steel H-piles oriented with the major axis resisting longitudinal bridge movements. The abutment fills are approximately 5.8m (19 ft) deep as measured from the top of the pile cap. The soil boring data indicated the underlying soil strata to be a very stiff clay. Limited soil data were available and the fills were assumed to be a stiff clay. The average pile length is 14.3m (47 ft) at the down station abutment and is 13.9m (45.5 ft) at the other abutment. Pertinent substructure properties are shown in Table 1.

A computerized reduction of weather data at Columbia, Missouri, for the period 1946 to 1965 yielded equations for both diurnal and hourly vari-

Table 2. Maximum Principal Stresses for Superstructure with Frictionless Bearings

h_c[a]	Mo.	Day	Slab								Beam							
			Hr	Vert[b]	Sta[c]	σ[d]	Hr	Vert[b]	Sta[c]	σ[d]	Hr	Vert[b]	Sta[c]	σ[d]	Hr	Vert[b]	Sta[c]	σ[d]
5.68	Jan.	17	4	t	33.60	3328	6	b	30.33	-6291	4	b	15.24	46884	2	b	0.0	-12135
5.68		18	4	t	1.52	3335	6	b	30.33	-6258	2	b	15.24	48401	2	b	0.0	-12273
28.38		17	2	t	30.33	3488	4	b	30.33	-6429	2	b	15.24	47160	2	b	0.0	-12204
28.38		18	2	t	36.88	3418	4	b	30.33	-6452	2	b	15.24	46333	2	b	0.0	-11997
5.68	July	19	16	b	30.33	5008	12	t	0.0	-4528	8	b	0.0	4413	18	t	30.33	-30751
5.68		20	16	b	30.33	5015	12	t	15.24	-4517	8	b	0.0	4275	18	t	30.33	-30268
28.38		19	16	b	30.33	4318	12	t	0.0	-3503	8	b	0.0	5171	18	t	0.0	-25166
28.38		20	16	b	30.33	4319	12	t	0.0	-3487	8	b	0.0	5033	18	t	0.0	-25235

Note: 1 W/m^2-°C = 0.17615 Btu/hr-ft^2-°F ; 1 m = 3.2808 ft ; 1 kN/m^2 = 0.14504 psi

[a] W/m^2-°C ; [b] t = top, b = bottom ; [c] m ; [d] kN/m^2

Table 3. Maximum Principal Stresses for Superstructure with Non-Integral Abutments

h_c[a]	Mo.	Day	Slab								Beam							
			Hr	Vert[b]	Sta[c]	σ[d]	Hr	Vert[b]	Sta[c]	σ[d]	Hr	Vert[b]	Sta[c]	σ[d]	Hr	Vert[b]	Sta[c]	σ[d]
5.68	Jan.	17	4	t	36.98	3328	6	b	30.33	-6291	4	b	15.24	48125	2	b	-0.15	-12135
5.68		18	4	t	0.00	3332	6	b	30.33	-6258	2	b	15.24	49573	2	b	-0.15	-12273
28.38		17	2	t	30.33	3488	4	b	30.33	-6429	2	b	15.24	48401	2	b	-0.15	-12204
28.38		18	2	t	31.96	3418	4	b	30.33	-6452	2	b	15.24	47643	2	b	-0.15	-11997
5.68	July	19	16	b	30.33	5008	12	t	-0.15	-4528	8	127.94	0.0	0	20	t	15.24	-33026
5.68		20	16	b	30.33	5015	12	t	15.24	-4517	8	127.94	0.0	0	18	t	15.24	-33715
28.38		19	16	b	30.33	4317	12	t	-0.15	-3503	8	130.18	-0.15	414	18	t	30.33	-26890
28.38		20	16	b	30.33	4319	12	t	-0.15	-3487	8	130.18	-0.15	276	18	t	30.33	-26890

Note: 1 W/m^2-°C = 0.17615 Btu/hr-ft^2-°F ; 1 cm = 0.3937 in. ; 1 m = 3.2808 ft ; 1 kN/m^2 = 0.14504 psi

[a] W/m^2-°C ; [b] t = top, b = bottom, distance in cm ; [c] m ; [d] kN/m^2

Table 4. Maximum Principal Stresses for Superstructure with Integral Abutments

h_c[a]	Mo.	Day	Slab								Beam							
			Hr	Vert[b]	Sta[c]	σ[d]	Hr.	Vert[b]	Sta[c]	σ[d]	Hr	Vert[b]	Sta[c]	σ[d]	Hr	Vert[b]	Sta[c]	σ[d]
5.68	Jan.	17	4	t	30.33	3328	4	b	30.33	-6210	4	b	30.33	46608	2	b	-0.15	-12135
5.68		18	4	t	0.00	3334	6	b	30.33	-6258	2	b	30.33	47850	2	b	-0.15	-12273
28.38		17	2	t	30.33	3488	4	b	30.33	-6429	2	b	30.33	46884	2	b	-0.15	-12204
28.38		18	2	t	33.60	3418	4	b	30.33	-6452	4	b	0.0	47091	2	b	-0.15	-11997
5.68	July	19	16	b	30.33	5008	12	t	-0.15	-4528	16	b	10.67	3172	16	b	0.0	-71706
5.68		20	16	b	30.33	5015	12	t	18.27	-4517	16	b	10.67	3240	16	b	0.0	-71706
28.38		19	16	b	30.33	4318	12	t	-0.15	-3503	8	b	-0.15	827	16	b	0.0	-61570
28.38		20	16	b	30.33	4319	12	t	-0.15	-3487	6	b	-0.15	620	16	b	0.0	-61570

Note: 1 W/m^2-°C = 0.17615 Btu/hr-ft^2-°F ; 1 m = 3.2808 ft ; 1 kN/m^2 = 0.14504 psi

[a] W/m^2-°C ; [b] t = top, b = bottom ; [c] m ; [d] kN/m^2

ations in ambient air temperature and the sum of direct and diffuse solar radiation incident upon a horizontal surface. From these equations, the maximum air temperature of 41°C (106°F) occurred on July 20 and the minimum air temperature of -23°C (-10°F) occurred on January 18. These temperatures can be expected to recur every 11 and 4.5 years for the maximum and minimum temperatures, respectively. The details of this study have been presented elsewhere (12).

Using the values obtained from the above weather equations as boundary conditions to the differential heat flow equation, a two-dimensional finite element analysis with the grid of Fig. 1e was used to calculate the distribution of temperature through the cross section of an interior composite-girder at two hour intervals over a two day period. These temperatures were then used to calculate the thermal stresses and horizontal forces induced in the structure.

The reference temperature at time of erection was assumed to be 7°C (45°F) for the temperature variations of July 19-20 and 32°C (90°F) for the temperature variations of January 17-18 (12).

For simplicity, it was assumed that soil deformations would be small and that the soil would behave as a linearily elastic material. The approach fill was considered to resist expansive movements only.

Partial Results

Reactions, deflections, slopes, strains, and stresses induced in a typical interior girder by environmental temperature extremes for the twenty year period, 1946-1965, were investigated for support conditions of a) frictionless bearings, b) non-integral abutments and c) integral abutments. To allow for a build up of dirt, a coefficient of static friction of 0.6 was assumed at the pier expansion bearings for cases b) and c). Thus, the force required to produce impending motion at the pier expansion bearings was 19,570 kg (43.2 kips). Both a nominal wind speed, h_c = 28.4 W/m^2 - °C (5 Btu/hr-ft^2 - °F) and no wind, h_c = 5.7 W/m^2-°C (1 Btu/hr-ft^2-°F) were combined with the hot days (July 19-20) and the cold days (January 17-18) weather exposures.

The interior girder was modeled with a composite-material slab-beam type element the formulation of which is presented elsewhere (12). The temperature on each horizontal plane was calculated by averaging the nodal point temperatures found from the finite element analysis. The slab temperatures over the width of the girder flange were assumed constant but different from that of the slab between girders.

The induced stresses for the three support conditions are shown in Tables 2, 3, and 4. Although the results clearly show that environmentally induced stresses are significant, the stresses induced by non-integral abutment type supports are approximately the same as that for frictionless bearings.

Table 5, the horizontal thrust results, shows that impending motion never occured at the expansion bearings.

Table 5. Maximum Horizontal Forces

h_c[a]	Mo.	Day	Hr.	Non-Integral		Integral	
				Abut.[b]	Pier[b]	Abut.[b]	Pier[b]
5.68	Jan.	17	6	23647	3171	22741	3216
5.68	Jan.	18	6	23556	3171	22695	3216
28.38	Jan.	17	4	24100	3216	23148	3262
28.38	Jan.	18	4	24145	3216	23194	3262
5.68	July	19	16	7112	2627	28403	2627
5.68	July	20	16	7067	2627	28403	2627
28.38	July	19	16	6206	2220	25368	2220
28.38	July	20	16	6161	2220	25368	2220

Note: 1 W/m^2-°C = 0.17615 Btu/hr-ft^2-°F ;

1 kg = 2.2075 lbs ; [a] W/m^2-°C ; [b] kg

Discussion of Results and Conclusions

A rational method is presented for placement of expansion bearings and bridge deck devices and for calculation of forces induced in bridge superstructures supported by flexible substructures.

For the composite-girder bridge structure located near Columbia, Missouri, even the most severe climatic conditions will not produce impending motion at the expansion bearings.

As the substructure stiffness increases and/or the bridge length increases, significant horizontal forces can develop in both non-integral and integral types of bridge structures. These forces can be reduced by orienting the abutment piling so that the minor axis (rather than the major) resists longitudinal movements. The calculated thrusts would also be less if nonlinear soil behavior were considered.

Abutment thrusts approached 7112 kg (15.7 kips) compression and 24,145 kg (53.3 kips) tension for the non-integral abutment and 28,403 kg (62.7 kips) compression and 23,194 kg (51.2 kips) tension for the integral abutment.

The maximum induced beam stresses are approximately 48,401 kN/m^2 (7.0 ksi), 49,573 kN/m^2 (7.2 ksi) and 71,706 kN/m^2 (10.4 ksi) for supports of frictionless bearings, non-integral abutments, and integral abutments, respectively. Slab stresses were significant and are approximately the same for each support condition. Based on this data, it can be seen that frictionless bearings and non-integral abutments yield beam stresses which are approximately 35 percent of the allowable whereas integral abutments yield beam stresses of 52 percent the allowable.

References

1. American Association of State Highway Officials, Standard Specifications for Highway Bridges, 11th ed., Washington, D. C., author, 1973.
2. Armaly, B. F., and Leeper, S. P., "Diurnal Stratification of Deep Water Impoundments," Paper No. 75-HT-35, presented at the AICHE-ASME Heat Transfer Conference, San Francisco, Calif., Aug. 11-13, 1975, American Society of Mechanical Engineers.
3. Beer, F. P., and Johnston, Jr., E. R., Mechanics for Engineers, Statics, and Dynamics, McGraw-Hill Book Company, Inc., New York, N. Y. 1957.
4. Berwanger, C., "Thermal Stresses in Composite Bridges," Proceedings, American Society of Civil Engineers, Specialty Conference on Steel Structures, Engineering Extension Series, No. 15, University of Missouri-Columbia, Mo., June 1970, pp. 27-36.
5. Emanuel, J. H., and Ekberg, C. E., Jr., "Problems of Bridge Supporting and Expansion Devices and an Experimental Comparison of the Dynamic Behavior of Rigid and Elastomeric Bearings, "Special Report," Project 547-S, Iowa State University, Iowa Engineering Experiment Station, Sept. 1965.
6. Emanuel, J. H., et al., "An Investigation of Design Criteria for Stresses Induced by Semi-Integral End Bents: Phase I--Feasibility Study," Missouri Cooperative Highway Research Program Final Report 72-9, University of Missouri-Rolla, 1973.
7. Emanuel, J. H., and Hulsey, J. L., "Thermal Stresses and Deformations in Nonprismatic Indeterminate Composite Bridges," Transportation Research Record 607, Transportation Research Board, Washington D. C., January 1976.
8. Emanuel, J. H., and Hulsey, J. L., "Prediction of the Thermal Coefficient of Expansion of Concrete," Journal of the American Concrete Institute, Proceedings, Vol. 74, No. 4, April 1977, pp. 149-155.
9. Emanuel, J. H. and Hulsey, J. L., "Temperature Distribution in Composite Bridges," Journal of the Structural Division, American Society of Civil Engineers, Vol. 104, No. ST1, Jan. 1978, pp. 65-78.
10. Emanuel, J. H. and Hulsey, J. L., "Estimation of Air Temperature Extremes," American Society of Heating Refrigerating and Air-Conditioning Engineers, Inc., ASHRAE Transactions, Vol. 84, Part 2, Albuquerque Meeting, Paper No. 999, June, 1978.
11. Higdon, A., and Stiles, W. B., Engineering Mechanics, Vector Edition, Volume 1: Statics, Prentice-Hall, Inc., Englewood Cliffs, N. J., 1962.
12. Hulsey, J. L., "Environmental Effects on Composite-Girder Bridge Structures," Unpublished Ph.D.